NASA Technical Memorandum 4108

Lateral Stability Analysis for X-29A Drop Model Using System Identification Methodology

David L. Raney and James G. Batterson
Langley Research Center
Hampton, Virginia

National Aeronautics and
Space Administration
Office of Management
Scientific and Technical
Information Division

1989

Summary

A 22-percent dynamically scaled replica of the X-29A forward-swept-wing airplane has been flown in radio-controlled drop tests at the Langley Plumtree Test Site. Flight data, which were recorded from early flights in the test program, consisted mainly of large-amplitude maneuvers over wide angle-of-attack ranges with several uncontrolled wing rock episodes. A system identification study of the recorded data was undertaken to examine the stability and control derivatives that influence the lateral behavior of this vehicle with particular emphasis on an observed wing rock phenomenon. All major lateral stability derivatives and the damping-in-roll derivative were identified for angles of attack from 5° to 80° by using a data-partitioning methodology and a modified stepwise regression algorithm. No control effectiveness derivatives could be identified from these first flights in the test program.

Introduction

Tests of dynamically scaled airplane models continue to be the most reliable source of information on high-angle-of-attack, flight dynamic characteristics prior to the actual flight tests of a particular airplane. A properly scaled dynamic model may be thought of as a simulator with the proper values of the various aerodynamic and inertial parameters. One such dynamic model test method, the radio-controlled drop model technique, involves dropping an unpowered, dynamically scaled model from a helicopter, flying it through a series of test maneuvers by remote control from the ground, and finally recovering it with a parachute. These tests can provide an important step toward understanding the dynamic characteristics of an airplane configuration since the testing is done in the actual flight environment. In addition, these models do not endanger a human pilot in an expensive airplane prototype. The emergence of good, miniature, instrumentation packages and telemetry systems makes it possible to measure and transmit air data, control surface deflections, and airplane responses to a ground station where they are recorded for later analysis.

Drop tests of a model of the X-29A forward-swept-wing airplane were conducted by the Langley Low-Speed Aerodynamics Division (LSAD). A purpose of these tests was to verify a wind-tunnel prediction of wing rock for angles of attack greater than 20°. In the first two data flights, violent lateral oscillations occurred in this angle-of-attack range, thus culminating in a roll departure. In order to ascertain the source of these severe rolling motions, the recorded data from those tests were provided to the Langley Guidance and Control Division where a system identification analysis was conducted. The purpose of this paper is to present the results of that analysis. A thorough description of the drop tests is presented in references 1 and 2.

First, the conduct of the drop test procedure and the system identification methodology that was applied to the flight data are described. Results of the analysis in the form of lateral stability and damping derivative estimates are then discussed and compared with wind-tunnel predictions from reference 3. Results of a validation scheme for checking the integrity of the estimates are also presented and discussed. A concluding section summarizes the most important results.

Symbols and Abbreviations

a_Y	lateral acceleration, g units
b	wing span
C_a	general aerodynamic force and moment coefficient
C_l	rolling-moment coefficient, $M_X/\bar{q}Sb$
C_n	yawing-moment coefficient, $M_Z/\bar{q}Sb$
C_Y	lateral-force coefficient, $F_Y/\bar{q}S$
$\bar{c}$	wing mean aerodynamic chord
F_Y	force along lateral body axis
g	acceleration due to gravity ($1g \approx 32.174$ ft/sec^2)
I_X, I_Y, I_Z	moments of inertia about longitudinal, lateral, and vertical body axes
J	cost function
$\ell+1$	number of parameters in regression equation
M_X, M_Z	rolling and yawing moments
N	number of data points in bin
p	roll rate, rad/sec or deg/sec
$\bar{q}$	dynamic pressure, $\rho V^2/2$
S	wing area
t	time, sec
V	free-stream velocity
x_i	independent variable (regressor) in regression equation
y	dependent variable (aerodynamic force or moment coefficient) in regression equation

α	angle of attack, deg or rad
$\dot{\alpha}$	rate of change of angle of attack, deg/sec or rad/sec
β	sideslip angle, deg or rad
δ_a	aileron deflection angle, deg or rad
δ_r	rudder deflection angle, deg or rad
θ_i	nondimensional stability or control derivative in regression equation
σ	standard deviation

Subscript:

0	bias term in regression equation

Abbreviations:

LSAD	Low-Speed Aerodynamics Division
MSR	modified stepwise regression
SAS	stability augmentation system
TED	trailing edge down
TEU	trailing edge up

A dot ($\dot{}$) over a symbol denotes a derivative with respect to time. A circumflex ($\hat{}$) denotes an estimated value.

Derivatives of aerodynamic coefficients $C_a (a = Y, l, n)$ referenced to a system of body axes with the origin at the airplane center of gravity:

$$C_{a_p} = \frac{\partial C_a}{\partial \frac{pb}{2V}} \qquad C_{a_{\delta_a}} = \frac{\partial C_a}{\partial \delta_a}$$

$$C_{a_\beta} = \frac{\partial C_a}{\partial \beta} \qquad C_{a_{\delta_r}} = \frac{\partial C_a}{\partial \delta_r}$$

Flight Vehicle Description and Drop Test Procedure

Flight data were generated during drop tests of an unpowered, 22-percent dynamically scaled replica of the forward-swept-wing X-29A research airplane. The model is equipped with controllable flaperons, rudder, canard, and strake flaps as depicted in figure 1. The flaperons act both symmetrically and differentially for lift and roll, respectively. Canard and strake flap deflections are purely symmetric for pitch control. The model is unpowered with the result that no fuel is burned and the center-of-gravity location is constant throughout the flight. A summary of the mass and geometry characteristics of the model is presented in table I.

Drop tests are conducted at the Langley Plumtree Test Site. A schematic representation of the drop test procedure is presented in figure 2. (See ref. 1.) A helicopter carries the model to an altitude of approximately 6000 ft and then releases it for a radio-controlled descent. The overall model control loop consists of downlinked flight data, a digital computer on which the control laws are implemented, and a command uplink. The pilot, who sits at a control station monitoring data displays and a video image of the model, provides three-axis commands through a customized control box. The instrumentation package of the model measures angle of attack, angle of sideslip, airspeed, linear accelerations, angular rates, and control surface deflections. Data time histories are recorded at the rate of 100 samples per second. Recorded angular rates are numerically differentiated after the flight to obtain angular accelerations. Flights are numbered sequentially by LSAD. This report presents parameter estimates based on data from flights 2, 3, 5, 6, 7, and 8. Data from flight 4 were obtained, but that flight consisted mainly of a well-developed spin; thus, the information content of those data was insufficient for the estimation of lateral stability parameters.

Flights 2 and 3 operated with a longitudinal stability augmentation system (SAS) in effect and with virtually no lateral augmentation. These flights covered an angle-of-attack range from 5° to about 35°. With essentially no lateral SAS, a sudden onset of poorly damped, uncommanded rolling oscillations (wing rock) occurred as the model entered certain angle-of-attack ranges. The wing rock behavior of the model, which made control difficult at angles of attack greater than 20°, eventually resulted in a roll departure. The first set of parameter estimates presented in this paper is based on data from flights 2 and 3 and covers angles of attack up to 32°.

Flights 5, 6, 7, and 8 were conducted with longitudinal and lateral SAS operating, which permitted control of the vehicle to much higher angles of attack. Wing rock oscillations were suppressed, and data were produced at angles of attack up to 80° during pull-up maneuvers. The second set of parameter estimates presented in this paper is based on data from these flights for angles of attack between 30° and 80°. None of the flight data analyzed in this report consisted of maneuvers designed specifically for parameter estimation purposes. Therefore, the flights did not contain simple control doublets and pulses that are necessary for a straightforward estimation of control effectiveness derivatives. No control effectiveness derivatives could be consistently identified from these flights. A summary of several

important characteristics associated with each flight is presented in table II.

Analytical Methods

A system identification study typically addresses two problems. The first problem involves model structure determination, and the second problem involves estimation of the parameters associated with terms included in the model. The system identification study described in this report utilized a regression technique to obtain parameter estimates from flight data. Prior to the regression procedure, a partitioning process was applied to the flight data.

Data Partitioning

The X-29A drop tests contained many transient and large-amplitude maneuvers over a wide angle-of-attack range. In order to produce stability parameter estimates that reflect the overall variation of the aerodynamic coefficients with angle of attack (α), a data-partitioning technique was employed. This technique permits the analysis of unplanned or uncontrolled large-amplitude maneuvers such as those experienced in flights 2 and 3. Data partitioning requires the sorting of data points into angle-of-attack bins, each of which covers a small angle-of-attack range (usually only 1° or 2°). A single bin will contain data from all portions of the maneuver during which the model was in that particular angle-of-attack range. These portions of flight data do not have to be, and often are not, contiguous in time. Figure 3 illustrates the manner in which a single maneuver may be partitioned into several bins on angle-of-attack space (α space). This process is thoroughly described and demonstrated in reference 4.

The regressional analysis (to be discussed below) employs a simple curve-fitting algorithm and does not require data that are contiguous in time. Since continuity in time for data in a particular bin is not needed, it is possible to combine data from separate maneuvers or even from separate flights into a single bin. In this way, information from several flights can be analyzed in one data set. The α dependence of the data in each bin is removed since the α range of each bin is small. Any bin that appears to retain some dependence may be broken into smaller bins if an adequate number of data points remain in each bin. This partitioning procedure, which has generally been applied on α space, may also be applied with respect to any other variable desired.

The partitioning of a maneuver that covers a large angle-of-attack range in a short period of time tends to yield a large number of bins that contain few data points. This was particularly true of maneuvers in flights 5, 6, 7, and 8 during which the lateral SAS was in effect, thus permitting controlled flight over a much broader α range than in flights 2 and 3. In order to produce a sufficient number of data points for regressional analysis on each bin, it was necessary to combine like bins from separate maneuvers and flights. An example of this is shown in figure 4 which illustrates the manner in which two separate maneuvers from flights 2 and 3 produced a data ensemble that contained sufficient points to create 2° bin sizes on an angle-of-attack range from 19° to 31°. Maneuvers from flights 5, 6, 7, and 8 were combined to produce an ensemble of 3° bin sizes on an α range from 30° to 80°. Estimates for lateral-directional stability and roll damping on these two α ranges will be presented and discussed in this report.

Modified Stepwise Regression

Once the partitioning has been completed, the parameter estimation may be conducted for each bin. In this study, an equation error method referred to as modified stepwise regression (MSR) was employed as a means of model structure determination and parameter estimation. The MSR algorithm (ref. 5) is a modification of linear regression which can approximate the structure of aerodynamic model equations and estimate the model parameters. When the analysis is conducted separately for each bin of partitioned data, the MSR yields a series of parameter estimates that reveal trends with respect to angle of attack. MSR successively enters a new independent variable (regressor) one at a time into a regression equation. Each new regressor is selected from a list of candidate variables established by the user before initiation of the regression procedure.

The general form of a regression equation for an aerodynamic model can be expressed as the polynomial expansion

$$y(t) = \theta_0 + \theta_1\, x_1(t) + \ldots + \theta_n\, x_n(t)$$

where $y(t)$ represents an aerodynamic force or moment coefficient, $x_j(t)$ represents a regressor consisting of an airplane output or control variable (or some combination thereof), and θ_j represents the stability or control derivative associated with the regressor $x_j(t)$. The new regressor is selected from the list of candidate variables based on the correlation of its time history with that of the aerodynamic coefficient $y(t)$. Values for parameters θ_j are obtained by minimizing the cost function J_{SR} defined as

$$J_{SR} = \sum_{i=1}^{N} \left[y(i) - \theta_0 - \sum_{j=1}^{\ell} \theta_j\, x_j(i) \right]^2$$

where N equals the number of data points in the bin being analyzed and $(\ell + 1)$ is the number of parameters in the current regression equation. This cost function represents the least-squares difference between the measured value of the aerodynamic coefficient (based on sensor data) and the predicted value of the aerodynamic coefficient (based on the current regression model). The "best" parameter estimates for θ_j will be those that minimize this cost function. The iterative process of adding regressors to the aerodynamic model, and then estimating the new parameters associated with those regressors (and the ones previously in the model), allows one to assess the impact of each new addition to the model and its ability to predict the given aerodynamic coefficient. In each step of the process, all terms in the regression are evaluated for their significance in minimizing the cost function, and those found insignificant according to a statistical selection criterion are deleted. The process continues until no new regressors are selected from the list of candidate variables. In applications to actual flight data, the final model produced in this manner may be overparameterized; thus, criteria for selecting an adequate model from an earlier step in the regression have been developed and are discussed in reference 6. A more detailed description of modified stepwise regression may be found in references 5, 6, and 7, which also include information relating to the use of this algorithm on a digital computer.

Results and Discussion

Estimates of lateral-directional stability derivatives for the X-29A drop model have been obtained from the six-flight data ensemble that was partitioned on α space. The combined estimates cover an α range from 5° to 80°. Estimates from flights 2 and 3, which cover an α range from 5° to 35°, are presented in figures 5 and 6 (solid symbols). Open symbols, for comparison, represent wind-tunnel data from a 16-percent-scale model of the X-29A that was tested in the Langley 30- by 60-Foot Tunnel (ref. 3). The wind-tunnel data used for comparison were taken for the model with control settings of the canard at −25°, the flap at 17.5°, and the strake at 30°. Several discrepancies are seen between wind-tunnel and flight test results for $\alpha > 20°$. These may arise because the dynamics of the flight maneuvers give rise to time-dependent phenomena that are not evident in static wind-tunnel tests. Evidence of similar discrepancies (although both are correct measurements for their respective tests) is given in references 8 and 9. The estimates for C_{n_β} confirm the wind-tunnel prediction that directional stability is retained to at least $\alpha = 30°$. Since wing rock episodes occurred at angles of attack as low as 17°, this result indicates that loss of directional stability is not a causal factor in the initiation of wing rock. A decrease in directional stability is observed for $\alpha = 15°$ and above in figure 5. This drop in C_{n_β} may arise from a blanketing effect of the fuselage and wing wake upon the vertical fin in this angle-of-attack region. The estimates for C_{l_β} show a slightly lower (but still stable) negative dihedral effect than was predicted by the wind tunnel.

Estimates for roll damping in figure 6 indicate a region of unfavorable damping for angles of attack between 17° and 24°. Another region of unfavorable damping exists for angles of attack greater than 27°. The existence of unfavorable roll damping is a likely cause of the wing rock oscillations observed in these α ranges. Wind-tunnel investigations have revealed that the loss of roll damping is caused by a pronounced asymmetry of fuselage forebody vortices under a rolling condition. (See ref. 3.) It is interesting to note that C_{l_β} remains negative throughout the regions of unfavorable roll damping, thus indicating that wing rock is a dynamic instability manifested by a statically stable system.

A close examination of the data from flights 2 and 3 reveals that two angle-of-attack regions of differing wing rock behavior can be defined. By plotting sideslip angle β versus roll rate p for wing rock episodes from these two flights, it becomes apparent that the oscillations are limit cycles at certain times and divergent cycles at others. The limit-cycle oscillations are indicated by the closed circular patterns at the center of the phase plane plots in figure 7. Divergent oscillations are indicated by the outward expanding spirals. Each segment of wing rock data shown in figure 7 exhibits these two regions of oscillation. Examination of these patterns revealed that all limit-cycle oscillations occurred at angles of attack between 17° and 27°. Above 27°, the wing rock oscillations are divergent. The roll-damping estimates from figure 6 reinforce the existence of these trends. Because essentially no lateral SAS was operational in flights 2 and 3, these data represent the "natural" behavior of the vehicle with no control action taken to suppress the wing rock oscillation.

Estimates of lateral-directional stability derivatives for $\alpha = 30°$ to 80° are presented in figures 8 and 9. These estimates (solid symbols) are based on flights 5, 6, 7, and 8. A constant offset of approximately 0.6 is observed between wind-tunnel and flight estimates for C_{Y_β}. The character of the two curves is identical, although the constant offset persists throughout the angle-of-attack range. The development of this offset may be observed in the

estimates of C_{Y_β} for $\alpha = 5°$ to 35° in figure 5. The offset starts at $\alpha \approx 24°$ and reaches a value of about 0.6 at $\alpha = 32°$. It then persists throughout the remainder of angles of attack shown in figure 8. The appearances of this offset in two independent sets of parameter estimates tend to corroborate one another. No cause was found for this discrepancy.

The estimates for C_{l_β} on $\alpha = 30°$ to 80° show some offset from wind-tunnel predictions. Negative (favorable) dihedral effect is confirmed up to $\alpha = 80°$. The flight data indicate a slightly less negative value than was observed in the wind tunnel for $\alpha = 30°$ to 65°, but the data agree well for $\alpha = 65°$ to 80°.

The estimates for C_{n_β} at $\alpha = 30°$ to 80° based on the drop tests indicate a loss of directional stability at $\alpha = 34°$ (fig. 8). This may represent the culmination of the blanketing effect on the vertical fin that was observed to begin at about $\alpha = 14°$ in figure 5. The flight estimates indicate less directional stability than was observed in the wind tunnel. Wind-tunnel data indicate a reestablishment of static directional stability above $\alpha = 40°$, whereas flight estimates indicate that directional instability persists; however, a slight trend toward recovery is observed between $\alpha = 50°$ and 65°. Reestablishment of directional stability in the wind-tunnel tests was credited to the unusual vortex aerodynamics associated with the long slender forebody and flat elliptical cross section of the X-29A at high angle of attack. (See ref. 3.) This factor may be the cause of the trend toward C_{n_β} recovery between $\alpha = 50°$ and 65° that was observed in the estimates of drop test parameters. If so, the effect does not appear to be as pronounced in flight as was observed in the wind tunnel. It is possible that the drop model does not maintain static conditions long enough for the fuselage vortices to develop completely and take their full effect. This discrepancy between wind tunnel and flight estimates for directional stability in the poststall regime should be investigated in subsequent flights of the X-29A drop model.

Since many of the maneuvers in flights 5, 6, 7, and 8 consisted of rapid pull-ups through the regions of unfavorable roll damping, the dynamics associated with changing angle of attack were considered in producing the parameter estimates. To include a consideration of these dynamics, the flight data were partitioned with respect to the sign of $\dot{\alpha}$ as well as the magnitude of α. The more selective bins contained fewer data points, and therefore they contained less information for the regression using MSR. Subsequent application of the modified stepwise regression produced a slightly better fit of the flight data than did previous estimates. Estimates of C_{l_p} for $\dot{\alpha} > 0$ and $\dot{\alpha} < 0$ from flight data are compared with wind-tunnel predictions of C_{l_p} in figure 9. The values of C_{l_p} for $\dot{\alpha} > 0$ indicate less favorable roll damping than for $\dot{\alpha} < 0$. Wind-tunnel predictions lie roughly between the two sets of estimates. This disparity between estimates of C_{l_p} for $\dot{\alpha} > 0$ and $\dot{\alpha} < 0$ in the angle-of-attack range between 30° and 80° indicates that dynamic conditions are giving rise to hysteresis in the vehicle behavior with respect to angle of attack. The estimates of a less favorable C_{l_p} for $\dot{\alpha} > 0$ than for $\dot{\alpha} < 0$ suggest that the vehicle is more prone to wing rock episodes while α is increasing through the critical angle-of-attack ranges rather than decreasing. This observation of hysteresis with $\dot{\alpha}$ is of particular significance, since it indicates that the parameter estimation techniques employed herein may be capable of quantifying the effects of a somewhat elusive phenomenon such as dynamic stall if given adequate flight test data. A greater tendency toward wing rock was noted in the drop tests during pitch-up segments of maneuvers in the higher angle-of-attack ranges. Estimates of the static lateral-directional stability derivatives C_{Y_β}, C_{l_β}, and C_{n_β} were essentially identical for the conditions of $\dot{\alpha} > 0$ and $\dot{\alpha} < 0$. Tables III to V present a numerical listing of the estimates of stability derivatives from figures 5 to 9. A summary of the estimates of lateral stability parameters for the angle-of-attack range from 0° to 80° is presented in figures 10 and 11.

Validation

A good check on the validity of parameter estimates obtained from a system identification study is to use the estimates to predict the forces and moments which act on the flight vehicle. The following section describes the manner in which predicted time histories of the drop model behavior based on the parameter estimates were compared with predictions based on wind-tunnel data. Both sets of predictions were plotted against actual time histories of the vehicle behavior based on telemetered flight data.

Method

Time histories for the coefficients C_Y, C_l, and C_n have been computed and compared as a means of checking the integrity of parameter estimates. Three sets of time histories were computed for each coefficient. First, time histories of force and moment coefficients were computed from flight data using the telemetered measurements from accelerometers and differentiated rate gyros onboard the vehicle. These values represent measurements of the actual forces and moments experienced by the model during a

flight. Time histories for the force and moment coefficients were also computed based on simplified aerodynamic models using wind-tunnel estimates of the lateral stability parameters. Coefficient time histories were then computed from the same simplified aerodynamic models using drop test estimates of the lateral stability parameters that were generated by the MSR algorithm with data partitioning. The simplified models used to compute the side-force and moment coefficients are as follows:

$$C_Y(t) = C_{Y,0} + C_{Y_\beta}[\alpha(t)]\ \beta(t) + C_{Y_{\delta_r}}[\alpha(t)]\delta_r(t)$$

$$C_l(t) = C_{l,0} + C_{l_\beta}[\alpha(t)]\ \beta(t) + C_{l_p}[\alpha(t)]p(t)\frac{b}{2V} + C_{l_{\delta_a}}[\alpha(t)]\delta_a(t)$$

$$C_n(t) = C_{n,o} + C_{n_\beta}[\alpha(t)]\ \beta(t) + C_{n_{\delta_r}}[\alpha(t)]\delta_r(t)$$

Note that the stability coefficients are functions of $\alpha(t)$ and are obtained from interpolation of the parameter estimate summaries shown in figures 10 and 11. The control derivative estimates $C_{Y_{\delta_r}}$, $C_{n_{\delta_r}}$, and $C_{l_{\delta_a}}$ are taken from reference 10, and the same estimates are used in calculating both drop test and wind-tunnel coefficients. A comparison of time histories obtained from stability parameter estimates with the actual time histories provides a general indication of the integrity of the parameter estimates. An example of a side-force-coefficient time history is shown in figure 12. Figure 12(a) compares coefficient predictions based on wind-tunnel parameter estimates with the measured coefficient values (solid line). Figure 12(b) compares coefficient predictions based on MSR parameter estimates from drop tests with the measured coefficient values. Figure 12(c) shows the angle-of-attack time histories which correspond to the coefficient comparisons in figures 12(a) and 12(b). These allow the reader to determine the original parameter estimates from figures 10 and 11 that were used to compute the coefficients.

Figures 12 and 13 present time history comparisons for the side-force coefficient C_Y from two separate flight segments. The wind-tunnel estimates appear to underpredict the amplitude of the side-force oscillations that were observed during these portions of the drop tests. Note that the time histories cover an angle-of-attack range of approximately 0° to 60° in these two particular flight segments. The time histories shown indicate that the estimates of system identification parameter, which were derived from a partitioned data ensemble from several flights, provide a good ability to predict the vehicle behavior during a particular flight maneuver.

Figure 14 presents another side-force-coefficient time history. This maneuver includes a higher angle-of-attack range than the previous two. At approximately 11 sec into this maneuver, the angle of attack exceeded 50°. Wind-tunnel predictions of the coefficient C_Y apparently produced the wrong sign on the side-force oscillations observed in this time segment. Reviewing the wind-tunnel estimates of C_{Y_β} in figure 10 reveals that a change in the sign of this parameter was, in fact, predicted at approximately $\alpha = 50°$. This wind-tunnel prediction of positive C_{Y_β} apparently does not coincide with the actual behavior of the drop model. The overall agreement between the system identification predictions and the measured coefficient time history is somewhat poorer than in the two previous maneuvers, thus suggesting that the simplified model being used for C_Y is less adequate at these higher angles of attack.

Figures 15 and 16 present time histories for the rolling-moment coefficient C_l. It appears that the system identification predictions provide better agreement with the measured coefficient values at the peaks of the rolling-moment oscillations. This improvement is particularly apparent in figure 16 during the interval between 13 and 18 sec. Angles of attack during this interval lie within the range wherein data were partitioned with respect to the sign of $\dot{\alpha}$ as well as to the magnitude of α. This distinction as to the dynamic condition of angle of attack may be responsible for the improved prediction of rolling moment at the peaks of the oscillations. The simplified model used appears to provide a relatively good agreeement even in the higher angle-of-attack ranges.

A comparison of yawing-moment time histories is presented in figure 17. Most of the flights contained poor yaw excitation. The primary parameter influencing the yawing coefficient C_n is the directional stability derivative C_{n_β}. For the particular flight segment shown in figure 17, it appears that the wind-tunnel estimates mispredict the sign of the yawing-moment oscillations. The angle-of-attack range for which this occurs (approximately 55° to 80°) corresponds with the range in which wind-tunnel estimates predicted a recovery of directional stability, whereas the drop test estimates predicted a continued loss of directional stability (fig. 10). Apparently, this recovery of directional stability did not occur during the flight of the drop model.

Conclusions

Estimates of lateral-directional stability parameters and roll-damping parameter have been calculated using modified stepwise regression on flight data from drop tests of a 22-percent-scaled replica

of the X-29A forward-swept-wing research airplane. Data partitioning was used to obtain trends in aerodynamic parameters with angle of attack. Data from the first two flights were used to obtain parameter estimates that covered a range of angle of attack α from 5° to 35° and showed relatively good agreement with wind-tunnel measurements. Retention of directional stability was confirmed up to $\alpha = 30°$, and a slightly less negative dihedral effect was observed than was predicted from wind-tunnel tests. Estimates of the variation of rolling-moment coefficient with roll rate (C_{l_p}) indicate a loss of favorable roll damping at $\alpha = 17°$ that is followed by a brief recovery of damping for $\alpha = 24°$ to 27°; then, unfavorable damping occurs again for $\alpha > 27°$. These successive changes in roll-damping character appear to give rise to two differing types of wing rock behavior. The first is a limit-cycle oscillation for angles of attack between 17° and 27°. The second is a divergent oscillation at angles of attack greater than 27°.

Estimates were also made based on data from four flights covering an angle-of-attack range from 30° to 80°. A constant negative offset from wind-tunnel predictions was observed in estimates for the variation of side-force coefficient with sideslip angle (C_{Y_β}). Estimates for the variation of rolling-moment coefficient with sideslip angle (C_{l_β}) showed very good agreement with wind-tunnel measurements. The configuration is statically stable in roll up to $\alpha = 80°$. Significantly lower directional stability was observed than that predicted by wind-tunnel tests. The configuration loses directional stability at $\alpha = 34°$ and remains unstable or marginally stable for all angles of attack above this value. Estimates for C_{l_p} were produced by partitioning with respect to the sign of the rate of change of angle of attack ($\dot{\alpha}$) as well as to the magnitude of angle of attack. Resulting values for roll damping indicate less favorable C_{l_p} for $\dot{\alpha} > 0$ than for $\dot{\alpha} < 0$. Therefore, a greater tendency toward wing rock is expected when α is increasing rather than decreasing. The dynamic condition of angle of attack appears to give rise to this hysteresis in the behavior of the X-29A drop model. A validation scheme was devised to investigate the ability of these parameter estimates to predict the actual behavior of the drop model. A better predictive capability was found when compared with predictions based on wind-tunnel estimates. This validation exercise presents the following general conclusions:

1. Both wind-tunnel measurements and system identification estimates provide reasonable predictions of the forces and moments which act on the model in the low-to-mid angle-of-attack range.

2. Simplified math models used in the validation exercise to predict the forces and moments acting on the model become less adequate as angle of attack becomes larger.

3. System identification parameter estimates appear to reflect the forces and moments which act on the drop model at high angles of attack more closely than wind-tunnel measurements.

NASA Langley Research Center
Hampton, VA 23665-5225
March 13, 1989

References

1. Fratello, David J.; Croom, Mark A.; Nguyen, Luat T.; and Domack, Christopher S.: Use of the Updated NASA Langley Radio-Controlled Drop-Model Technique for High-Alpha Studies of the X-29A Configuration. *A Collection of Technical Papers—AIAA Atmospheric Flight Mechanics Conference*, Aug. 1987, pp. 305–317. (Available as AIAA-87-2559.)
2. Croom, Mark A.; Whipple, Raymond D.; Murri, Daniel G.; Grafton, Sue B.; and Fratello, David J.: *High-Alpha Flight Dynamics Research on the X-29 Configuration Using Dynamic Model Test Techniques.* SAE Tech. Paper Ser. 881420, Oct. 1988.
3. Murri, Daniel G.; Nguyen, Luat T.; and Grafton, Sue B.: *Wind-Tunnel Free-Flight Investigation of a Model of a Forward-Swept-Wing Fighter Configuration.* NASA TP-2230, 1984.
4. Batterson, James G.; and Klein, Vladislav: Partitioning of Flight Data for Aerodynamic Modeling of Aircraft at High Angles of Attack. *A Collection of Technical Papers—AIAA Atmospheric Flight Mechanics Conference*, Aug. 1987, pp. 444–451. (Available as AIAA-87-2621.)
5. Klein, Vladislav; Batterson, James G.; and Murphy, Patrick C.: *Determination of Airplane Model Structure From Flight Data by Using Modified Stepwise Regression.* NASA TP-1916, 1981.
6. Batterson, James G.: *Estimation of Airplane Stability and Control Derivatives From Large Amplitude Longitudinal Maneuvers.* NASA TM-83185, 1981.
7. Klein, Vladislav; and Batterson, James G.: *Determination of Airplane Model Structure From Flight Data Using Splines and Stepwise Regression.* NASA TP-2126, 1983.
8. O'Leary, C. O.; and Drew, W.: *Flow Visualization on Rolling Models Using Minitufts.* Tech. Memo. 2083, British Royal Aircraft Establ., 1986.
9. Batterson, James G.: System Identification Applied to a Free-Flight Drop Model. *Paper presented at the 8th IFAC/IFORS Symposium on Identification and System Parameter Estimation* (Beijing, P. R. China), Aug. 27–31, 1988.
10. Budd, Gerald D.: *Locally Linearized Longitudinal and Lateral-Directional Aerodynamic Stability and Control Derivatives for the X-29A Aircraft.* NASA TM-84919, 1984.

Table I. Summary of Mass and Geometric Characteristics of X-29A Drop Model

Weight, lb	276.5
Moment of inertia:	
I_X, slug-ft^2	3.83
I_Y, slug-ft^2	43.62
I_Z, slug-ft^2	43.56
Wing:	
Span, ft	5.98
Mean aerodynamic chord, ft	1.58
Area, ft^2	8.96
Aspect ratio	4.0
Sweep (leading edge), deg	−29.27
Sweep (quarter-chord), deg	−33.73
Taper ratio	0.404
Dihedral angle, deg	0
Flaperon area (total), ft^2	1.39
Flaperon deflection, deg	17.5 (TED) to −27.7 (TEU)
Canard:	
Span, ft	3.0
Area (total), ft^2	1.79
Aspect ratio	1.47
Taper ratio	0.318
Deflection, deg	30 (TED) to −60 (TEU)
Vertical tail:	
Height, ft	1.47
Area, ft^2	1.63
Aspect ratio	1.33
Taper ratio	0.306
Rudder area, ft^2	0.335
Rudder deflection, deg	±30
Strake flap:	
Area (total), ft^2	0.504
Deflection, deg	±30

Table II. Summary of Flight Characteristics

Flight	Range of α, deg, on which derivatives were identified	Stability augmentation in effect	Description of flight
1	Not used	Longitudinal; very weak lateral	General checkout flight
2	5–32	Longitudinal; very weak lateral	Shallow pull-ups, turns, wing-rock-induced departure
3	5–32	Longitudinal; very weak lateral	Shallow pull-ups, turns, wing-rock-induced departure
4	Not used	Longitudinal; wing rock suppression	Well-developed spin, wing rock suppression
5	30–80	Longitudinal; wing rock suppression; spin suppression	Steep pull-ups, turns, spin prevention
6	↓	↓	↓
7			
8			

Table III. Estimates of Modified Stepwise Regression for Lateral-Directional Stability Derivatives With Standard Deviations

α, deg	C_{Y_β}		C_{l_β}		C_{n_β}	
	Estimate	σ value	Estimate	σ value	Estimate	σ value
8	−0.954	0.014	0.030	0.002	0.233	0.004
12	−.848	.012	.036	.002	.266	.003
16	−.807	.016	−.084	.003	.221	.004
18	−.831	.030	−.073	.004	.188	.003
20	−1.050	.027	−.102	.003	.168	.003
22	−1.350	.049	−.099	.004	.150	.004
24	−1.170	0.042	−0.118	0.004	0.113	0.004
25	−.612	.060	−.134	.004	.088	.006
26	−.700	.017	−.142	.003	.089	.004
27	−.700	.020	−.114	.003	.071	.005
28	−.696	.039	−.147	.003	.073	.011
30	−.720	.048	−.134	.004	.042	.016
32	−0.740	0.046	−0.126	0.006	0.036	0.011
34	−.798	.037	−.122	.006	.015	.012
37	−1.060	.049	−.153	.008	−.076	.018
40	−1.110	.048	−.120	.006	−.107	.013
43	−.989	.027	−.145	.002	−.145	.012
46	−1.070	.022	−.210	.004	−.208	.011
49	−1.030	0.025	−0.170	0.004	0.007	0.012
52	−.560	.020	−.124	.004	−.114	.009
55	−.365	.042	−.127	.003	−.027	.009
58	−.110	.011	−.114	.004	−.087	.017
61	−.273	.013	−.116	.002	.043	.007
64	−.144	.020	−.132	.003	.002	.008
67	−0.314	0.019	−0.132	0.002	−0.181	0.007
70	−.550	.017	−.145	.002	−.148	.005
73	−.584	.019	−.136	.002	−.151	.005
76	−.476	.019	−.154	.003	−.208	.007
79	−.267	.029	−.176	.002	−.170	.009

Table IV. MSR Estimates of Roll Damping Derivative With Standard Deviations—Data Partitioned by Positive and Negative $\dot{\alpha}$

α, deg	C_{l_p} for $\dot{\alpha} > 0$		C_{l_p} for $\dot{\alpha} < 0$	
	Estimate	σ value	Estimate	σ value
8	−0.491	0.011	−0.491	0.011
12	−.362	.012	−.362	.012
16	−.191	.030	−.191	.030
18	0	.026	0	.026
20	.090	.018	.090	.018
22	.151	.035	.151	.035
24	0	0.028	0	0.028
25	−.128	.020	−.128	.020
26	−.108	.025	−.108	.025
27	−.103	.014	−.103	.014
28	.175	.020	.175	.020
30	.121	.017	.121	.017
32	0.023	0.024	−0.241	0.049
34	.058	.020	.211	.026
37	.652	.042	.050	.030
40	.552	.045	−.114	.042
43	.579	.035	.148	.040
46	.422	.023	.421	.020
49	0.030	0.023	0.009	0.028
52	.908	.035	−.086	.039
55	.556	.028	−.156	.027
58	.607	.025	−.159	.035
61	.758	.044	.711	.059
64	.438	.025	.198	.073
67	−0.017	0.018	−0.245	0.022
70	.070	.017	.196	.017
73	.461	.022	.100	.021
76	.179	.013	−.085	.018
79	.002	.015	.022	.015

Table V. Wind-Tunnel Estimates for Lateral-Directional Stability Derivatives

α, deg	C_{Y_β}	C_{l_β}	C_{l_p}	C_{n_β}
0	−1.150	0.072	−0.450	0.129
5	−1.200	.063	−.380	.206
10	−1.150	.014	−.440	.229
15	−.974	−.103	−.300	.218
20	−.630	−.160	−.050	.155
25	−.401	−.160	0	.072
30	−0.230	−0.201	0.200	0.049
35	−.115	−.201	.200	−.014
40	−.372	−.185	.050	−.072
45	−.343	−.281	.240	.018
50	.057	−.270	.340	.069
55	.343	−.206	.190	.095
60	0.401	−0.215	−0.140	0.372
65	.286	−.143	(a)	.329
70	.143	−.135	(a)	.014
75	.229	−.143	(a)	.227
80	.573	−.149	(a)	.441

[a]Data not available.

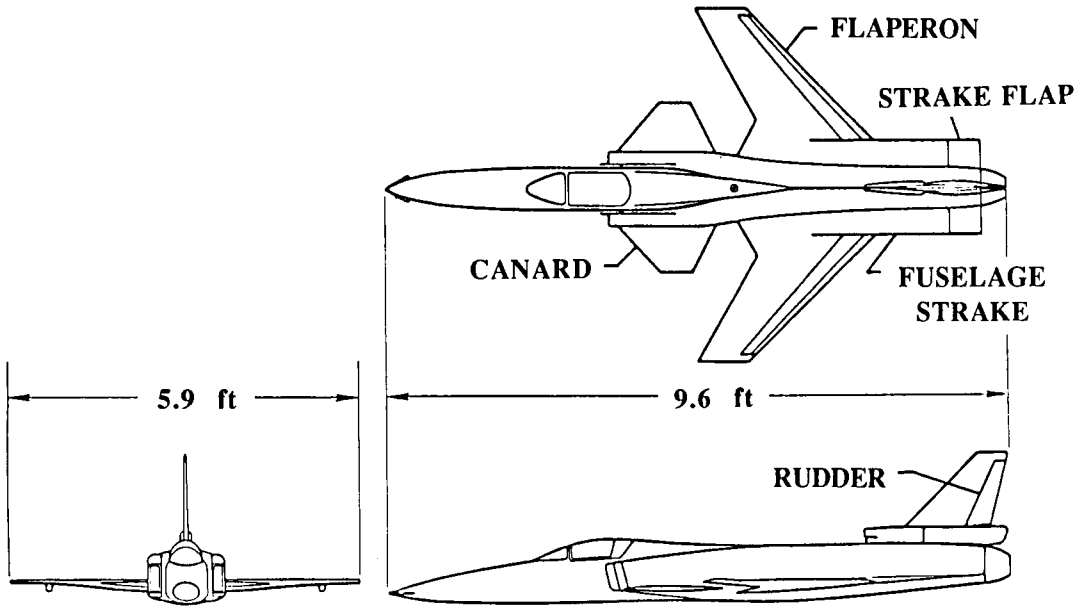

Figure 1. Radio-controlled X-29A drop model.

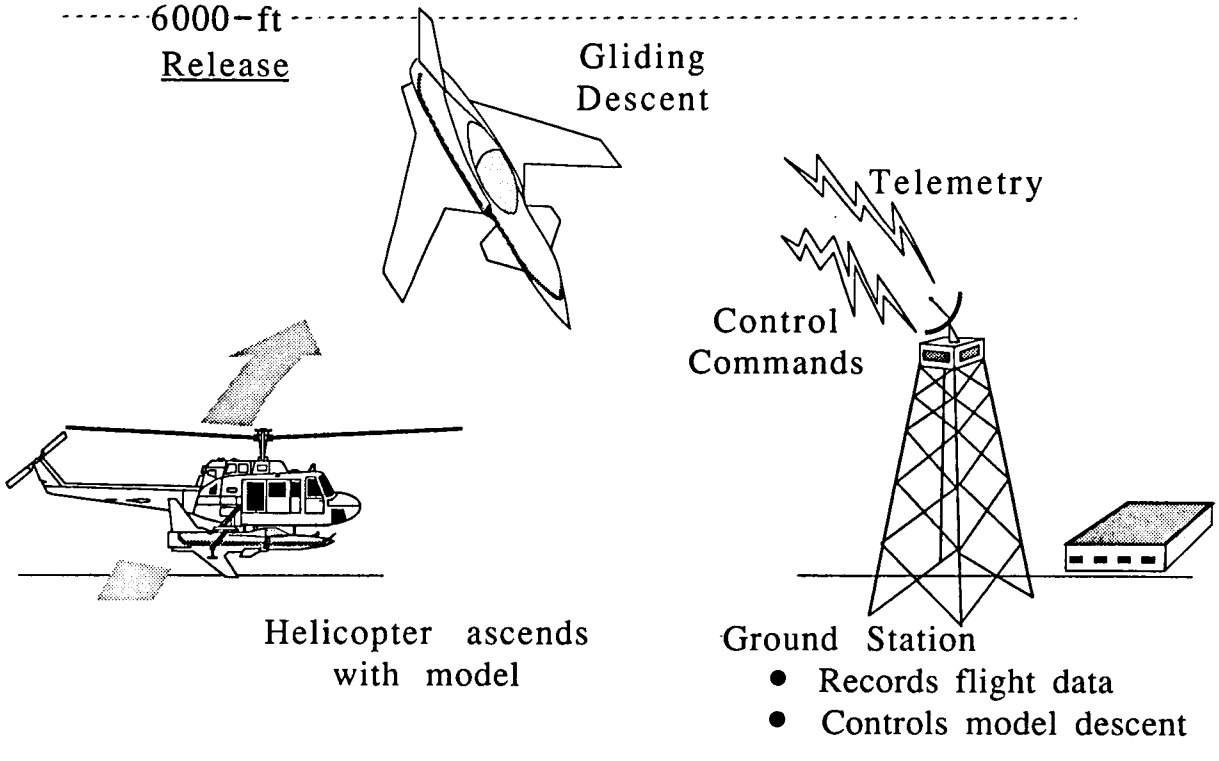

Figure 2. Schematic representation of drop test procedure.

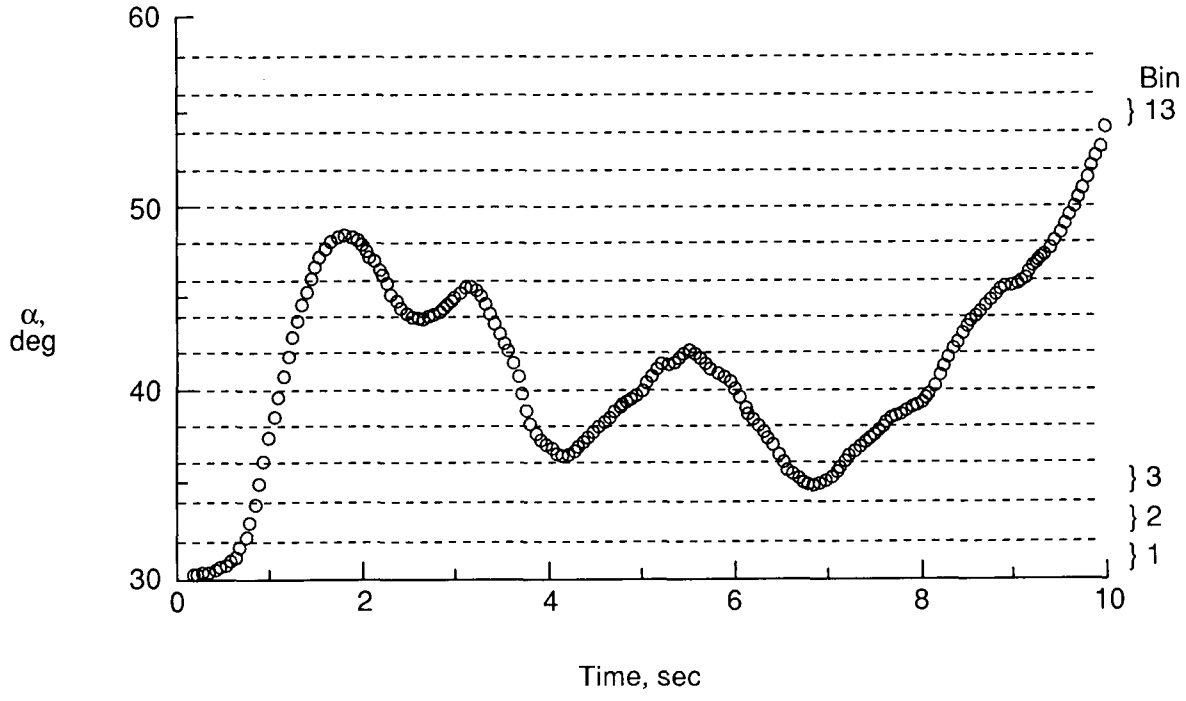

Figure 3. Example of partitioned data.

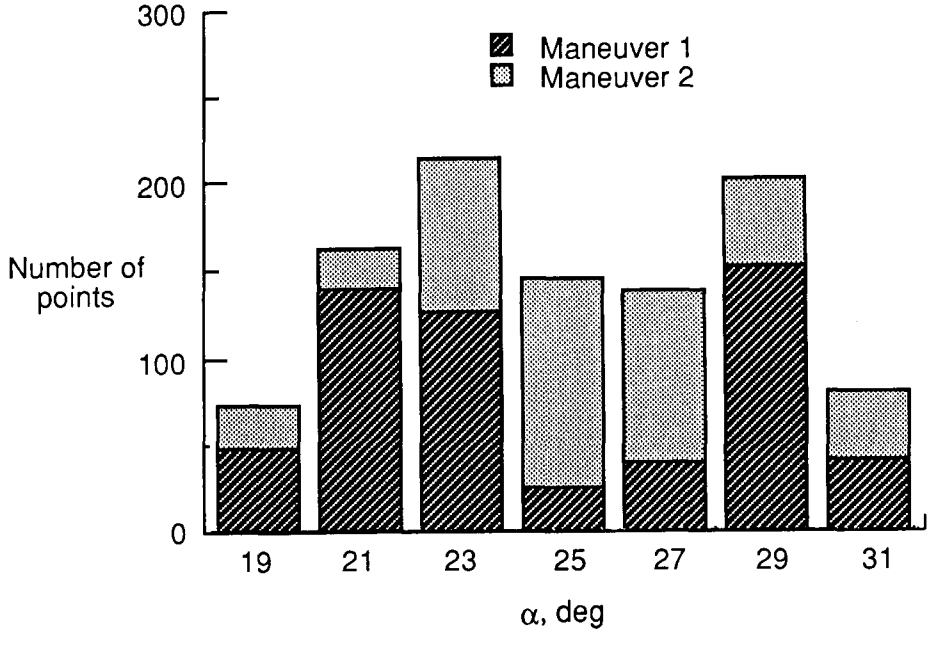

Figure 4. Combined maneuvers form data ensemble.

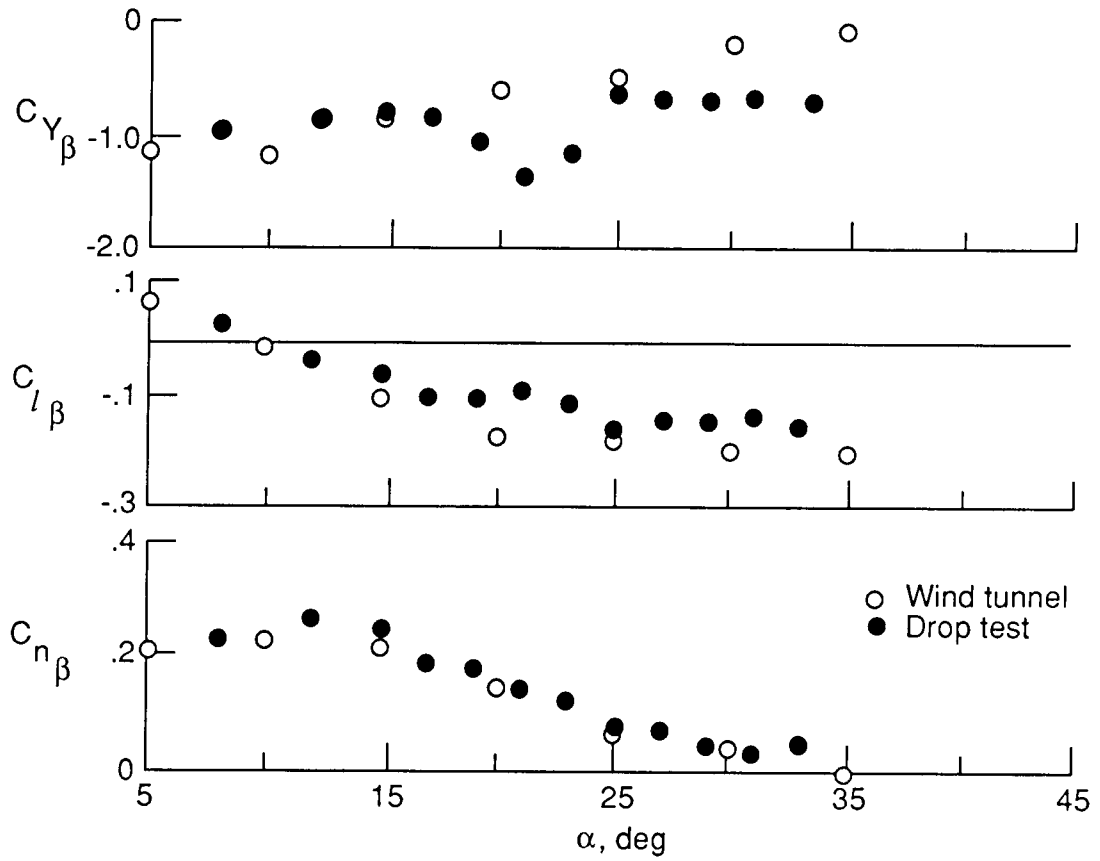

Figure 5. Comparison of lateral-directional stability derivatives for $\alpha = 5°$ to 35°.

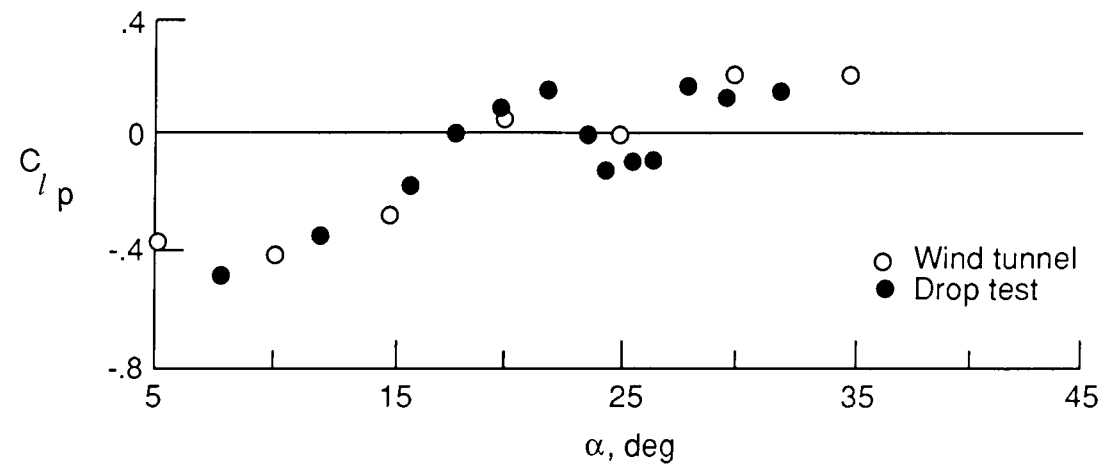

Figure 6. Comparison of roll-damping derivatives for $\alpha = 5°$ to 35°.

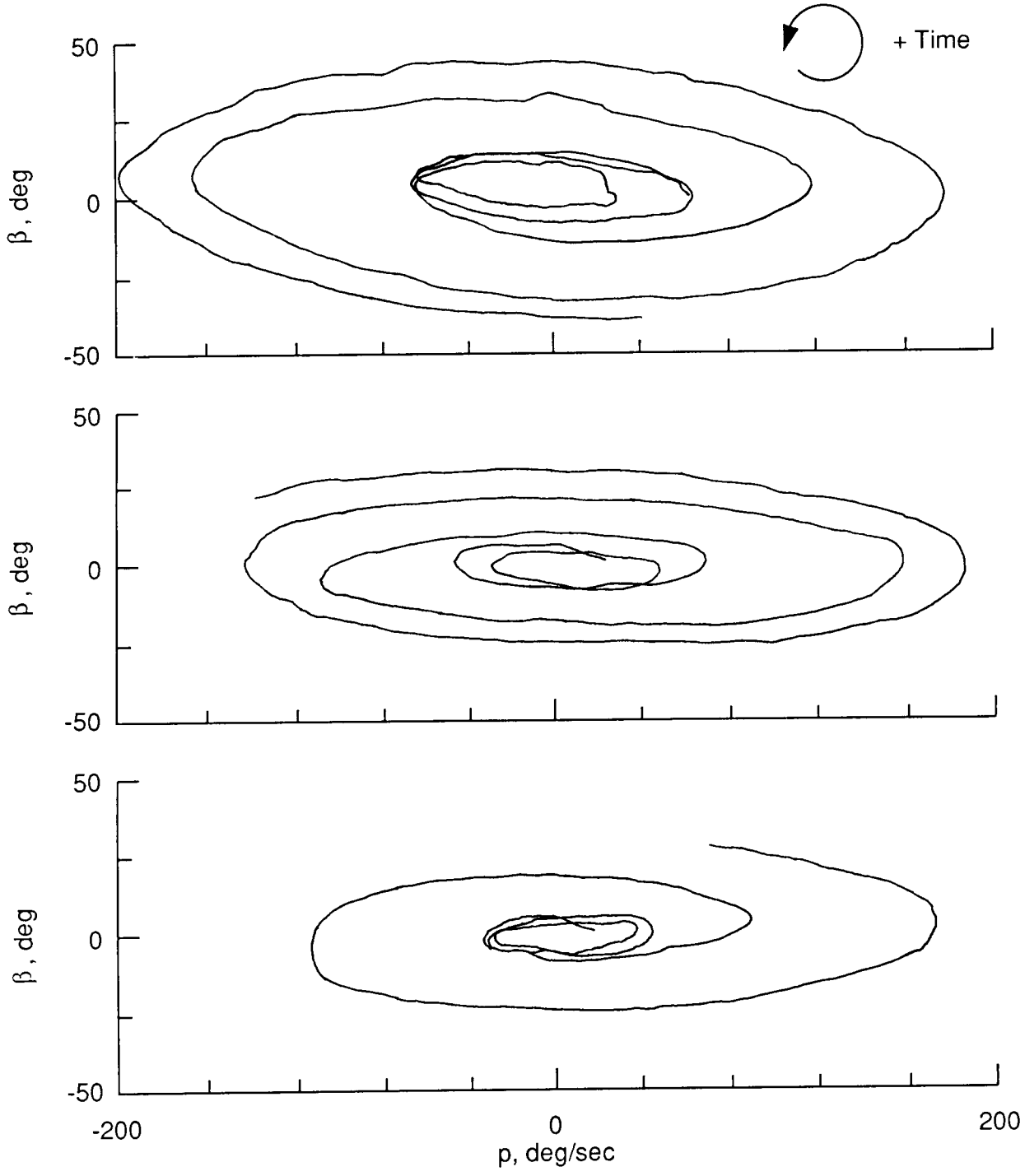

Figure 7. Data from several wing rock events.

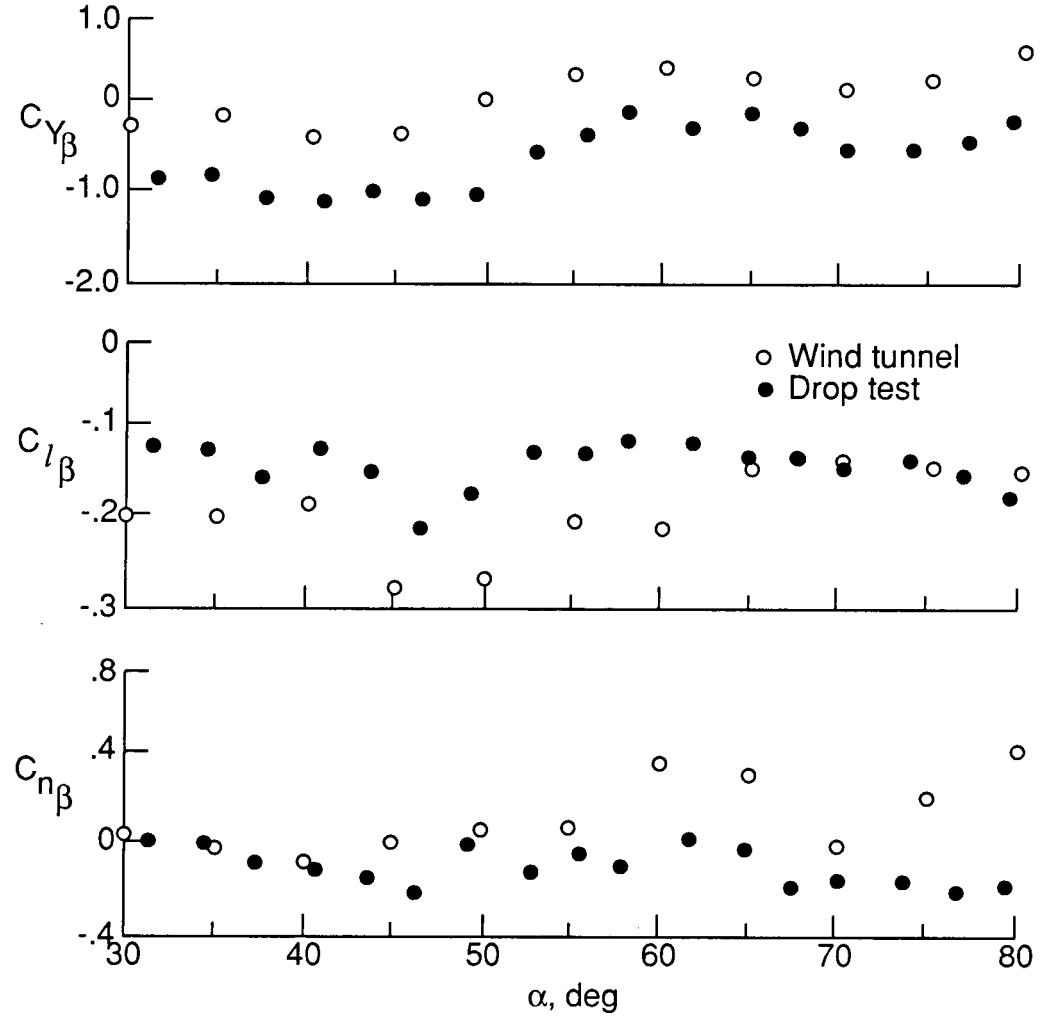

Figure 8. Comparison of lateral-directional stability derivatives for $\alpha = 30°$ to $80°$.

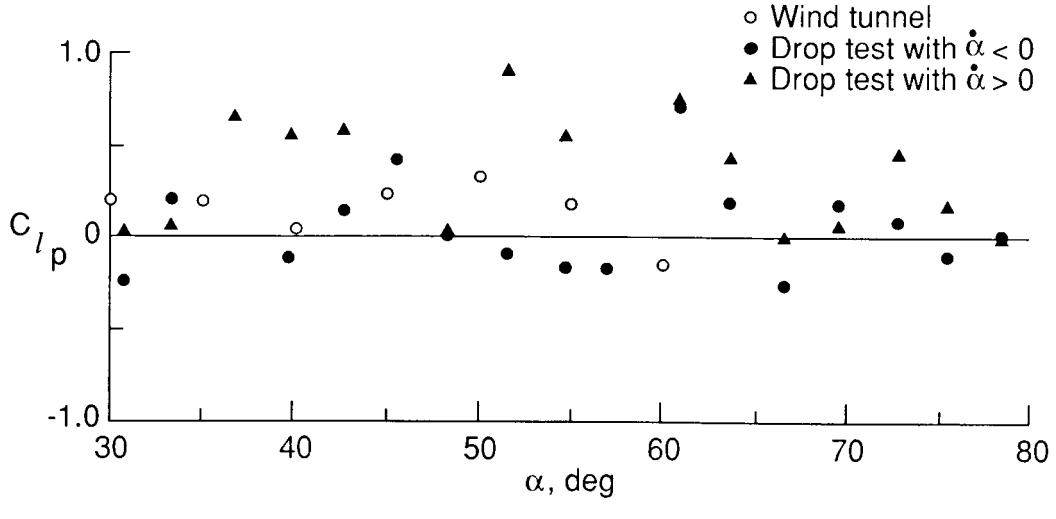

Figure 9. Comparison of roll-damping derivatives for $\alpha = 30°$ to $80°$.

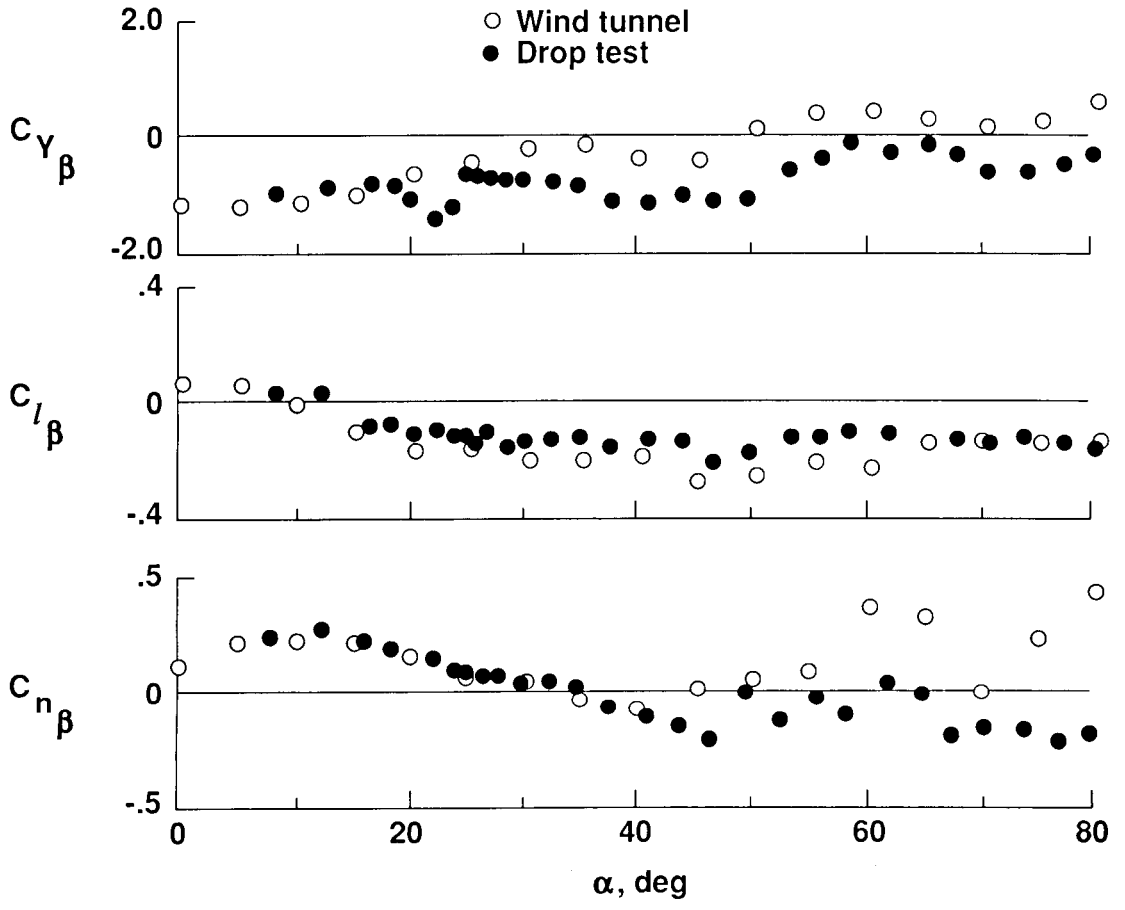

Figure 10. Combined lateral-directional stability derivative estimates for $\alpha = 0°$ to 80°.

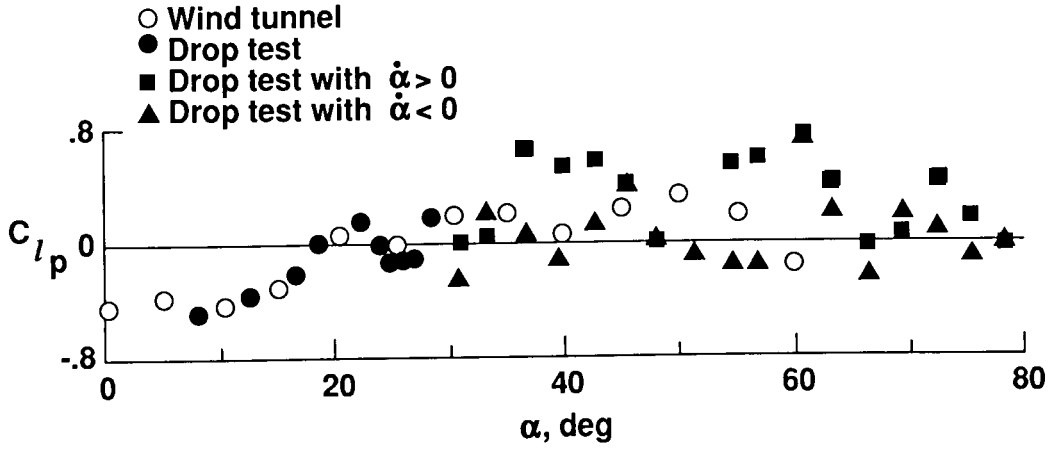

Figure 11. Combined roll-damping derivative estimates for $\alpha = 0°$ to 80°.

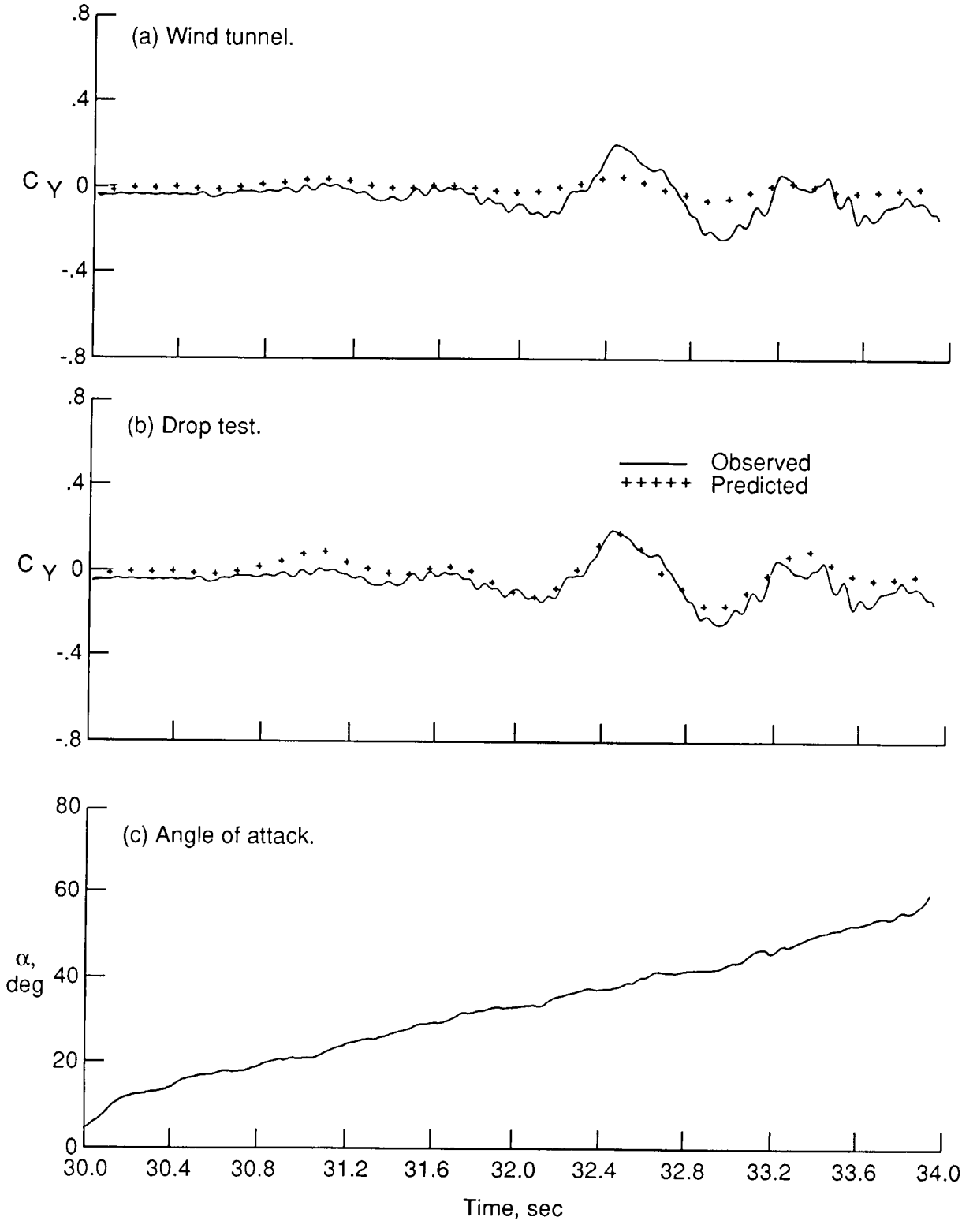

Figure 12. Validation plots of side-force coefficient for data segment from flight 5.

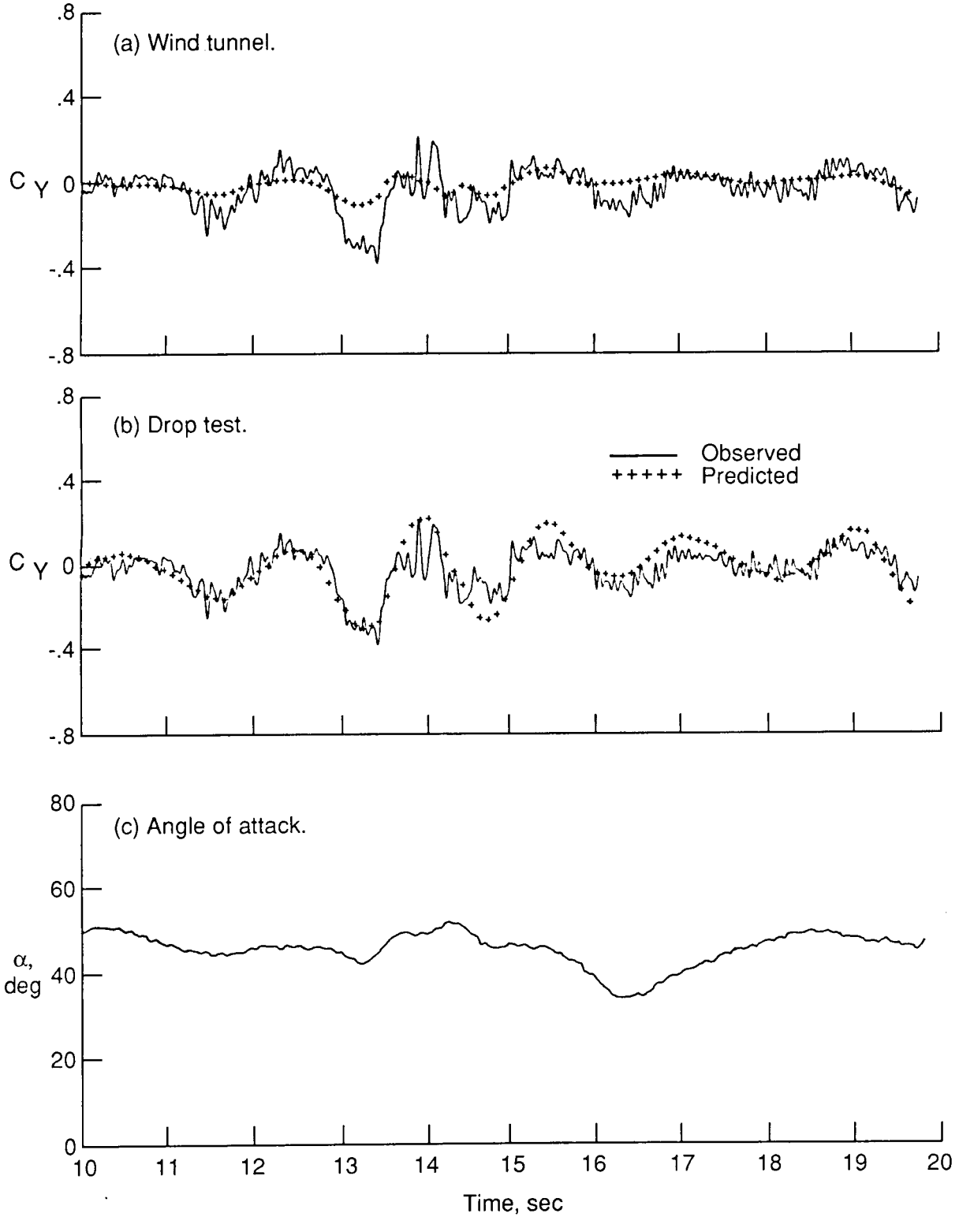

Figure 13. Validation plots of side-force coefficient for data segment from flight 7.

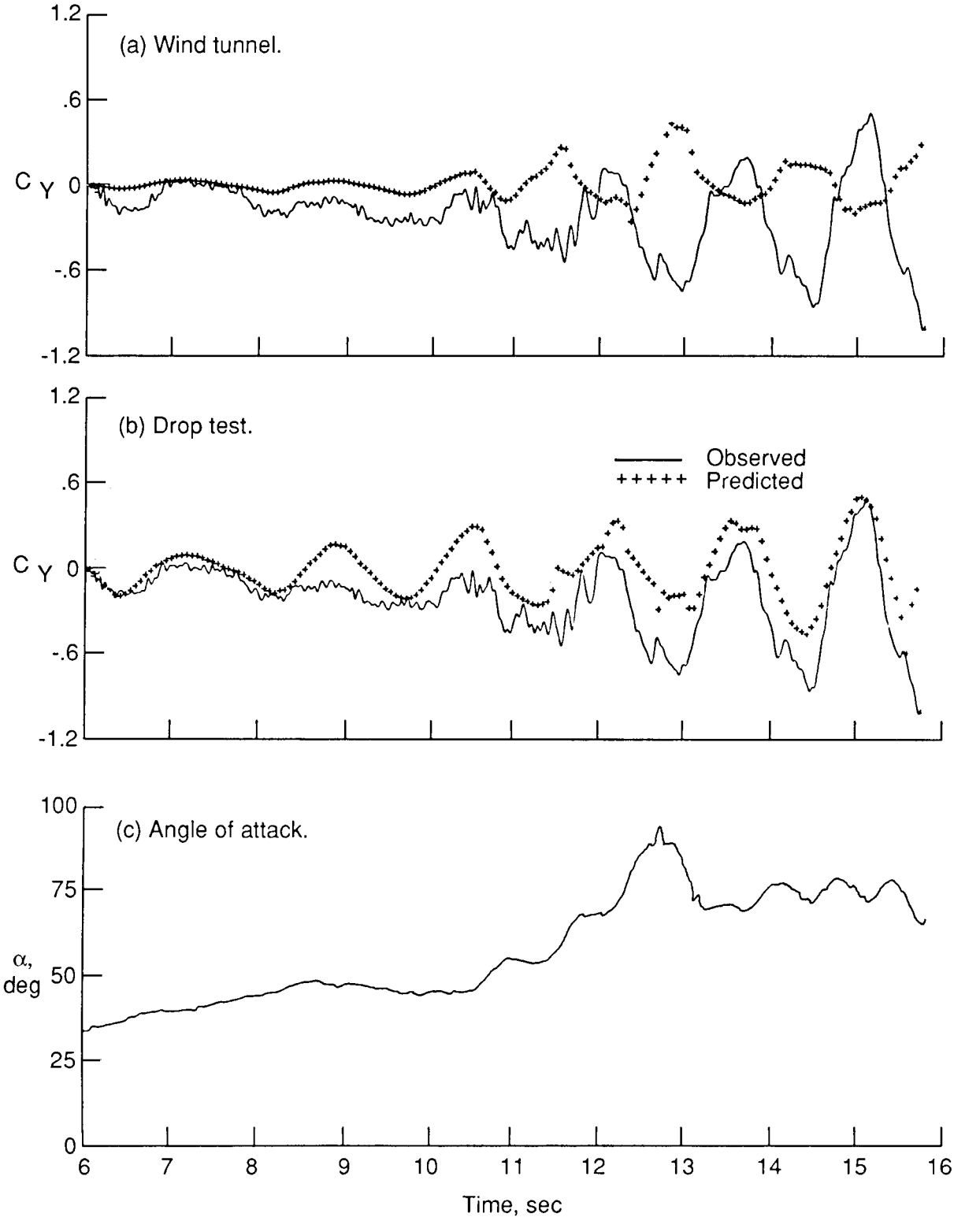

Figure 14. Validation plots of side-force coefficient for data segment from flight 8.

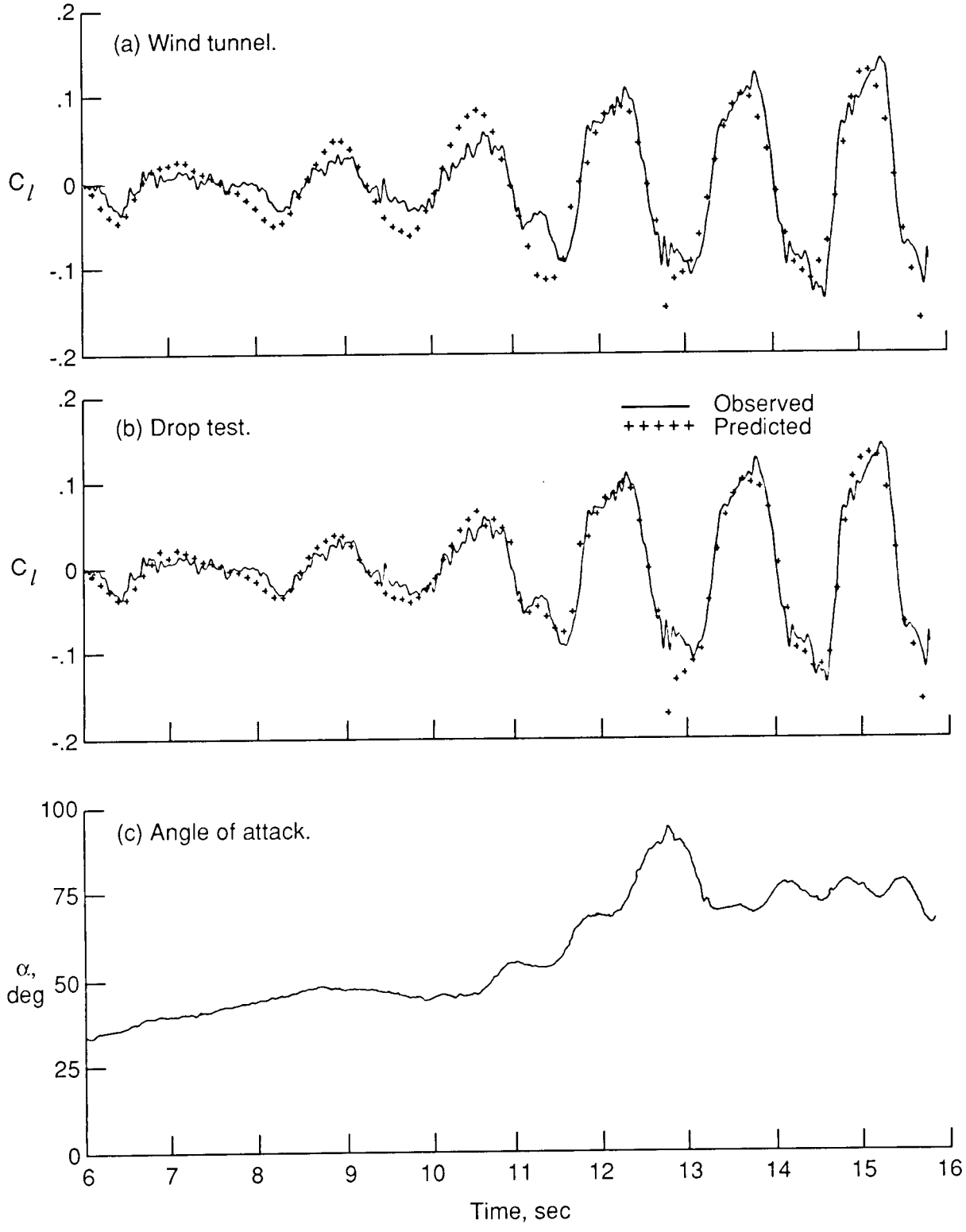

Figure 15. Validation plots of rolling-moment coefficient for data segment from flight 8.

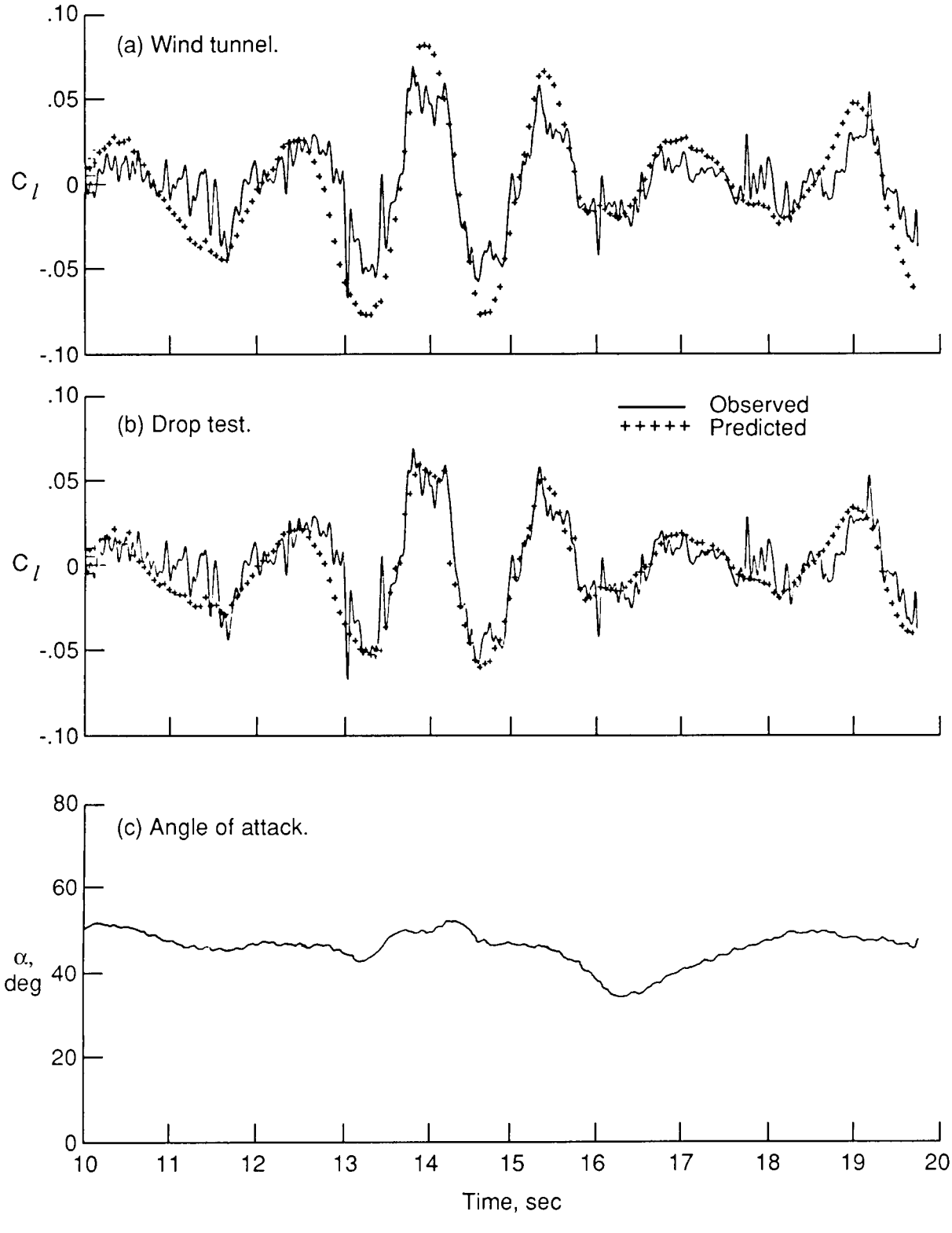

Figure 16. Validation plots of rolling-moment coefficient for data segment from flight 7.

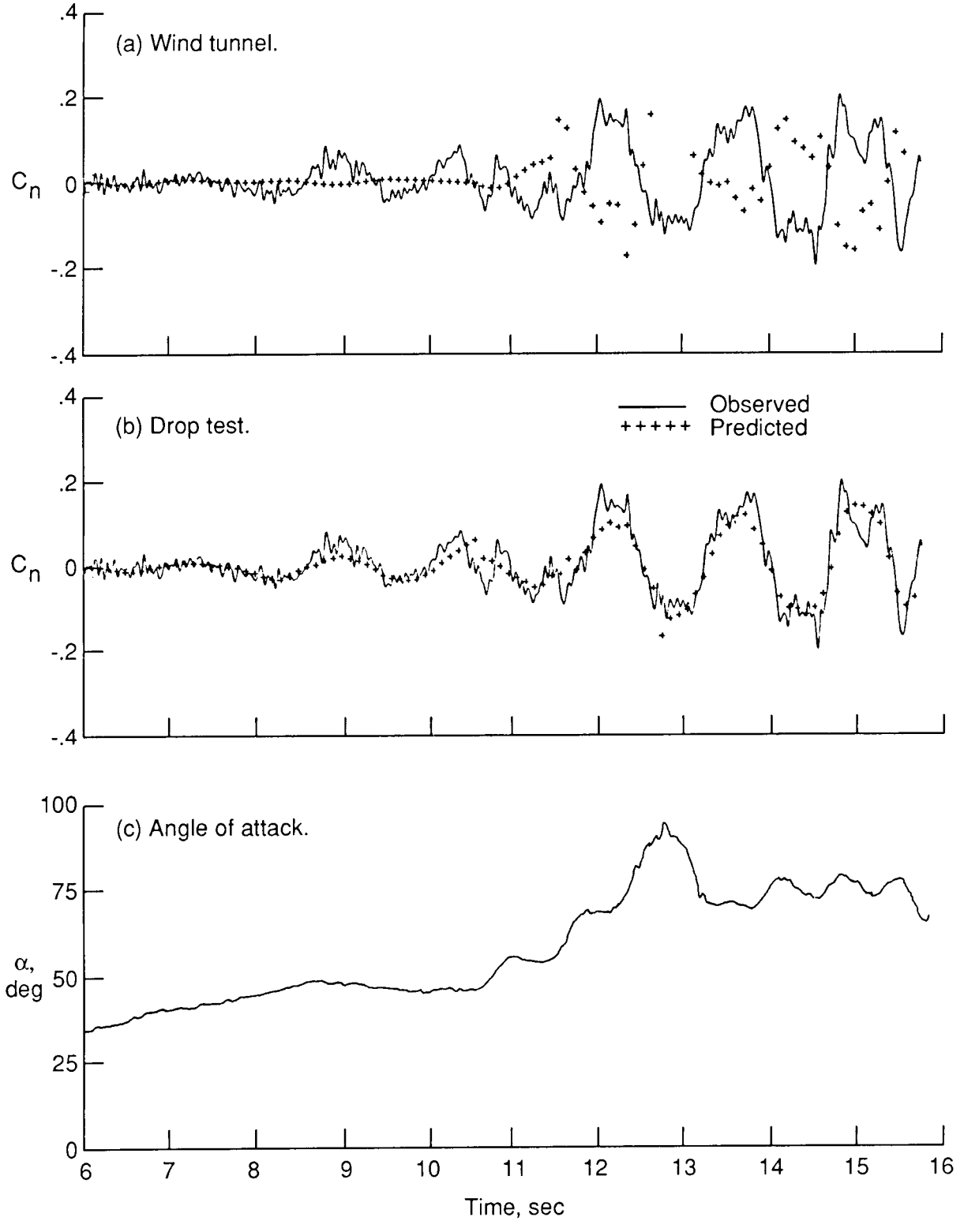

Figure 17. Validation plots of directional stability coefficient for data segment from flight 8.

NASA
National Aeronautics and Space Administration

Report Documentation Page

1. Report No.	2. Government Accession No.	3. Recipient's Catalog No.
NASA TM-4108		

4. Title and Subtitle	5. Report Date
Lateral Stability Analysis for X-29A Drop Model Using System Identification Methodology	June 1989
	6. Performing Organization Code
7. Author(s)	8. Performing Organization Report No.
David L. Raney and James G. Batterson	L-16471
9. Performing Organization Name and Address	10. Work Unit No.
NASA Langley Research Center Hampton, VA 23665-5225	505-66-01-02
	11. Contract or Grant No.
12. Sponsoring Agency Name and Address	13. Type of Report and Period Covered
National Aeronautics and Space Administration Washington, DC 20546-0001	Technical Memorandum
	14. Sponsoring Agency Code

15. Supplementary Notes

16. Abstract

A 22-percent dynamically scaled replica of the X-29A forward-swept-wing airplane has been flown in radio-controlled drop tests at the NASA Langley Research Center. A system identification study of the recorded data was undertaken to examine the stability and control derivatives that influence the lateral behavior of this vehicle with particular emphasis on an observed wing rock phenomenon. All major lateral stability derivatives and the damping-in-roll derivative were identified for angles of attack from 5° to 80° by using a data-partitioning methodology and a modified stepwise regression algorithm.

17. Key Words (Suggested by Authors(s))	18. Distribution Statement
X-29A drop model System identification Stepwise regression Wing rock	Unclassified–Unlimited Subject Category 08

19. Security Classif. (of this report)	20. Security Classif. (of this page)	21. No. of Pages	22. Price
Unclassified	Unclassified	25	A03

For sale by the National Technical Information Service, Springfield, Virginia 22161-2171